

*Proceedings  
of the Society  
for*

EXPERIMENTAL  
STRESS  
ANALYSIS

0348-2  
E2S  
V.40  
1983

0348-2  
E2S  
1983-2

8762724

0348-53  
5678  
1983



E8762724

Proceedings  
of the Society  
for

# EXPERIMENTAL STRESS ANALYSIS



VOLUME XL

---

K.A. Galione, Publisher  
M.E. Yergin, Editor



COPYRIGHT © 1983 BY SOCIETY FOR EXPERIMENTAL STRESS ANALYSIS  
14 FAIRFIELD DRIVE  
BROOKFIELD CENTER, CT 06805  
Printed in U.S.A., 1983

8762724

Proceedings  
of the Society  
for Experimental  
Stress Analysis





## SESA Executive Board

President  
J.B. LIGON  
Michigan Technological University

President-Elect  
W.N. SHARPE, JR.  
The Johns Hopkins University

Vice-President  
R.J. RINN  
Measurements Group, Inc.

Treasurer  
C.A. CALDER  
Oregon State University

Managing Director  
K.A. GALIONE  
SESA Headquarters

C.P. BURGER  
Iowa State University

S.K. FOSS  
John Deere Technical Center

R.H. MARLOFF  
Westinghouse R&D Center

S.E. SWARTZ  
Kansas State University

G.E. WARREN  
Naval Civil Engineering Laboratory

D.L. WILLIS  
Detroit Diesel Allison—GMC

W.M. MURRAY  
Honorary President

## Editorial Council

Chairman  
R.J. RINN  
Measurements Group, Inc.

Secretary  
K.A. GALIONE  
SESA Headquarters

P.H. ADAMS  
Sandia National Laboratories

D.G. BERGHAUS  
Georgia Institute of Technology

C.A. CALDER  
Oregon State University

D.A. DILLARD  
University of Missouri

B.C. DYKES  
The Boeing Company

S.K. FOSS  
John Deere Technical Center

D.H. MORRIS  
Virginia Polytechnic Institute  
and State University

J.W. PHILLIPS  
University of Illinois

G.E. WARREN  
Naval Civil Engineering Laboratory

J.B. LIGON  
Michigan Technological University  
*ex officio*

## Papers Review Committee

Chairman  
D.H. MORRIS  
Virginia Polytechnic Institute  
and State University

D.B. BARKER  
University of Maryland

C.W. BERT  
University of Oklahoma

G.L. CLOUD  
Michigan State University

W.H. PETERS III  
University of South Carolina

P.K. STEIN  
Stein Engineering Services, Inc.

J.L. TURNER  
Auburn University



Notice: The opinions expressed on the following pages are those of the individual authors and do not necessarily represent the ideas of the Society for Experimental Stress Analysis.

# Contents

Officers and Committees of the Society .....	vii
Dynamic Crack Curving—A Photoelastic Evaluation M. RAMULU AND A.S. KOBAYASHI	1
Measurements of Stresses, Forces and Moments on Nuclear Steam Generators M.T. FLAMAN AND N.N. SHAH	10
Displacement Measurements Around Cracks in Three-dimensional Problems by a Hybrid Experimental Technique C.W. SMITH, D. POST, G. HIATT AND G. NICOLETTO	15
Experimental Study of Inelastic Strain Patterns in a Model of a Tube-plate Ligament Using an Interferometric Moiré Technique C.A. WALKER, J. McKELVIE AND A. McDONACH	21
Epon 828 Epoxy: A New Photoelastic-model Material R.B. AGARWAL AND L.W. TEUFEL	30
A Rational Theory of Oblique Incidence and its Extension to Stress-Separation in Birefringent Composites SHIVE K. CHATURVEDI	36
Discussion of 'An Introduction to Dynamic Photoelasticity' J.A. CLARK AND A.J. DURELLI	42
On Stress Analysis of Anisotropic Composites Through Transmission Optical Patterns: Isochromatics and Isopachics K.A. JACOB, V. DAYAL AND B. RANGANAYAKAMMA	49
An Approximate Method of Orthotropic Photoelastic Analysis B.D. AGARWAL	55
A Method of Three-dimensional Strain Measurement on Non-ideal Objects Using Holographic Interferometry JOHN L. GOLDBERG	59
Experimental Technique for Measurement of Stress-acoustic Coefficients of Rayleigh Waves K. JASSBY AND D. KISHONI	74
In-Plane Shear Test of Thin Panels G.L. FARLEY AND D.J. BAKER	81
Transient Response of a Central Crack to a Tensile Pulse A.A. SUKERE AND W.N. SHARPE, Jr.	89
An Experimental Determination of the Fields of Strains and Stresses in the Elastoplastic Range S. RAUTU AND E. LEIBZON	99
The Iosipescu Shear Test as Applied to Composite Materials D.E. WALRATH AND D.F. ADAMS	105
Identification of Isochromatic Fringes A.J. DURELLI AND A. SHUKLA	111
Nondestructive Residual-stress Measurement in a Wide-flanged Rolled Beam by Acoustoelasticity H. FUKUOKA, H. TODA AND H. NAKA	120
Developments in the Design and Use of Liquid Metal Strain Gages J.E. STONE, N.H. MADSEN, J.L. MILTON, W.F. SWINSON AND J.L. TURNER	129
Simultaneous Measurements of Stress Intensity and Toughness for Fast-running Cracks in Steel D.A. SHOCKEY, J.F. KALTHOFF, W. KLEMM AND S. WINKLER	140
Fine-grid Method for Large Strain Analysis near a Notch Tip M. OBATA, H. SHIMADA AND A. KAWASAKI	146
A Hybrid Technique for Improved $K$ Determination from Photoelastic Data H.P. ROSSMANITH	152
Determination of Dynamic Properties of Elastomers Over Broad Frequency Range G.M. SMITH, R. BIERMAN AND S.J. ZITEK	158
Curvature Measurement by Moiré Effect R. RITTER AND R. SCHETTLER-KOEHLER	165

Strain Measurement with Asymmetric Oblique-incidence Polariscopes for Birefringent Coatings J. KOMOROWSKI AND J. STUPNICKI	171
Fracture Properties of Metals Under Rapid Heating and Loading N. DAGALAKIS, J.C.S. YANG AND H. YEH	177
The Monomode Fiber—A New Tool for Holographic Interferometry J.A. GILBERT, T.D. DUDDERAR, M.E. SCHULTZ AND A.J. BOEHNLEIN	190
Stress Analysis by Combination of Holographic Interferometry and Boundary-integral Method J. BALAS, J. SLÁDEK AND M. DRŽÍK	196
Discussion of 'An Analysis of Neutral Holes' R. RICHARDS, Jr. AND G.S. BJORKMAN, Jr.	202
Moiré Interferometry at VPI and SU DANIEL POST	203
Through-thickness Measurement of Residual Stresses in Thin Tubes J. DRUEZ AND A. BAZERGUI	211
Plane-stress Fracture Testing of Finite Sheets Under Biaxial Loads MICHAEL K. OLADIMEJI	217
Photoelastic Determination of Mixed-mode Stress-intensity Factors LAI ZHENGMEI AND SUN PING	228
A Semi-automated In-plane Loader for Materials Testing P.W. MAST, L.A. BEAUBIEN, M. CLIFFORD, D.R. MULVILLE, S.A. SUTTON, R.W. THOMAS, J. TIROSH AND I. WOLOCK	236
Crack-tip Stresses as Computed from Strains Determined by Stereo-imaging D.L. DAVIDSON, D.R. WILLIAMS AND J.E. BUCKINGHAM	242
Photoelastic Determination of Stresses in Multiple-pin Connectors M.W. HYER AND D.H. LIU	249
An Edge-cracked Mode II Fracture Specimen L. BANK-SILLS AND M. ARCAN	257
Determination of Stress-intensity Factors for Cracks in Tubes Under Torsion L.S. SRINATH, N. SRINIVASA MURTHY AND T.V. HAREESH	262
Another Method to Separate Principal Strains in Photoelastic Coatings PIETER J. SEVENHUIJSEN	268
A Case Study of the Seismic Response of Fluid-coupled-flexible Cylinders S.J. BROWN AND M. CHU	270
The Photoelastic-coating Technique for Plastic-elastic Contact H. FESSLER AND M. EISSA	282
Application of Fiber Optics to Speckle Metrology—A Feasibility Study T.D. DUDDERAR, J.A. GILBERT, A.J. BOEHNLEIN AND M.E. SCHULTZ	289
Influence of Late-breaking Ligaments on Crack Propagation in Compact Specimens— A Photoelastic Study A. SHUKLA AND J.W. DALLY	298
Half-fringe Photoelasticity: A New Approach to Whole-field Stress Analysis A. VOLOSHIN AND C.P. BURGER	304
Nonlinear Photoviscoelasticity: Theory and Measurement A. TOUGUI, D. GAMBY, A. LAGARDE AND H.F. BRINSON	314
A Noncontacting System for Measuring Effective Stress-Strain Curves of Ultra-thin X-ray-mask Materials T.D. DUDDERAR AND L.R. THIBAUT	322
Observation of Damage Growth in Compressively Loaded Laminates H. CHAI, W.G. KNAUSS AND C.D. BABCOCK	329
Hybrid Experimental-Numerical Stress Analysis ALBERT S. KOBAYASHI	338
Enhanced Displacement Measurement Using a Generalized Formulation for Double-aperture Specklegrams M.A. SUTTON, A. WONG AND Y.J. CHAO	348
A Technique for Cyclic-plastic Notch-strain Measurement M.W. GUILLOT AND W.N. SHARPE, Jr.	354
Measurement of Internal Strain in Cast-concrete Structures WILLIAM C. STONE	361



Slope Measurements Using Multiplexed Diffraction Gratings as Shearing Components in Interferometry M.A. SUTTON, Y.J. CHAO AND C.E. TAYLOR	370
Experimental Stress-intensity Distributions in Three-dimensional Cracked-body Problems C.W. SMITH, D. POST AND G. NICOLETTO	378
Discussion of 'On Stress Analysis of Anisotropic Composites Through Transmission Optical Patterns: Isochromatics and Isopachics' Y.J. CHAO, M.A. SUTTON AND C.P. HU	382
A High-strain Biaxial-testing Rig for Thin-walled Tubes Under Axial Load and Pressure D. LEFEBVRE, C. CHEBL, L. THIBODEAU AND E. KHAZZARI	384
Fragmentation of Metal Rings by Electromagnetic Loading D.E. GRADY AND D.A. BENSON	393
Reduction of Elastic Stress Concentrations in End-milled Keyed Connections M. EISSA AND H. FESSLER	401
The Effect of Preload on Fatigue Strength of Residually Stressed Specimens A.M. NAWWAR AND J. SHEWCHUK	409
Buckling of Cylinders with Cutouts Under Axial Compression SUSUMU TODA	414
A Highly Sensitive Noncontacting Electromagnetic Device for Detecting Dynamic Stresses in Structures G.N. REDDY AND S. SAHA	418
Fracture Behavior of Brittle Circular Rings Subjected to Concentrated Impulsive Loading S. KIDA AND J. ODA	425
Further Studies on Dynamic Crack Branching M. RAMULU, A.S. KOBAYASHI, B.S.J. KANG AND D.B. BARKER	431
A Consistent-splitting Model for Experimental Residual-stress Analysis E.F. RYBICKI, J.R. SHADLEY AND W.S. SHEALY	438
Discussion of 'The Moire' Method—A Review' AUGUST J. DURELLI	446
Loaded and Unloaded Optical Response of Polyester Model Material J.L.F. FREIRE, J.D. LAGE AND R.D. VIEIRA	450

# Dynamic Crack Curving—A Photoelastic Evaluation

by M. Ramulu and A.S. Kobayashi

**ABSTRACT**—A dynamic-crack-curving criterion, which is valid under pure Mode I or combined Modes I and II loadings and which is based on either the maximum circumferential stress or minimum strain-energy-density factor at a reference distance of  $r_0$  from the crack tip, is verified with dynamic-photoelastic experiments. Directional stability of a Mode I crack propagation is attained when  $r_0 = \frac{1}{128\pi} \left( \frac{K_I}{\sigma_{ox}} \right)^2 V_0^2 (C, C_1, C_2) > r_c$ , where  $r_c = 1.3$  mm for Homalite-100 used in the dynamic-photoelastic experiments.

## Introduction

Crack extension and fracture criteria under combined tension and shear loading are based on either energy or maximum circumferential-stress criteria. The maximum circumferential-stress,  $\sigma_{\theta\theta}$ , criterion was first used by Erdogan and Sih,<sup>1</sup> for predicting the direction,  $\theta_c$ , of an angled crack. Williams and Ewing<sup>2</sup> extended this theory by incorporating the second-order term of  $\sigma_{ox}$  in the Williams eigenfunction expansion. Finnie and Saith<sup>3</sup> corrected an oversight in the above angle crack analysis and obtained an improved agreement between predicted and experimental data. Streit and Finnie<sup>4</sup> further proposed a crack-stability model where directional stability of a Mode I crack propagation is maintained when a characteristic distance of  $r_0$  from the crack tip satisfies  $r_0 \geq r_c$ , where  $r_c$  is a critical distance ahead of the crack tip. Cotterell and Rice<sup>5</sup> derived the necessary condition for a slightly curved, quasi-static, mixed-mode crack growth where stability of crack growth was also governed by  $\sigma_{ox}$ . Karihaloo *et al.*<sup>6</sup> recently showed that crack curving can occur without kinking under vanishing  $\sigma_{ox}$  and Mode II stress-intensity factor, but with nonvanishing derivative of  $K_{II}$  with respect to the crack length.

As for the energy approach, Hussain *et al.*,<sup>7</sup> Palani-swamy and Knauss,<sup>8</sup> Gupta,<sup>9</sup> Wu,<sup>10</sup> and Nemat-Nasser *et al.*,<sup>11-12</sup> among others, predicted the direction of a kinked crack based on a maximum strain-energy release-rate criterion. Sih,<sup>13</sup> on the other hand, proposed the S-theory where the direction of crack kinking coincides with the direction of the minimum strain-energy density. Theocaris and Andrianopoulos<sup>14</sup> recently modified the S-theory by designating its mean value,  $\bar{S}$ , the critical quantity for crack initiation, under mixed-mode crack-tip deformation.

The above papers all relate to quasi-static crack extension. As for dynamic-crack-curving criterion, Yoffe<sup>15</sup> and Sih<sup>16</sup> used the maximum dynamic-circumferential-stress theory and minimum strain-energy-density theory, respectively, to explain crack-branching phenomena.

The objective of the present study is to derive a dynamic-crack-curving criterion applicable to both Mode I and combined Modes I and II crack-tip deformation. In particular, dynamic extensions of two modified static-crack-curving criteria, that is the maximum circumferential stress and the minimum strain-energy-density criteria at a critical distance  $r_c$ , were considered. The developed theoretical relations were evaluated numerically and the influence of  $\sigma_{ox}$  and crack velocity on crack-curving direction were deduced. Crack-curving angles predicted by the two dynamic-crack-curving criteria were then compared with experimental results, obtained from past dynamic-photoelastic investigation.

## Dynamic Crack-curving Criteria

### Elastodynamic-crack-tip Stress Field

The dynamic-crack-curving criteria are derived from the near-field, mixed-mode elastodynamic state of stress associated with a crack tip propagating at constant velocity. This dynamic state of stress is given by Freund<sup>17,18</sup> in terms of local rectangular and polar coordinates of  $(x, y)$  and  $(r, \theta)$ , respectively, with origin at the crack tip, and the Mode I and II dynamic-stress-intensity factors,  $K_I$  and  $K_{II}^*$ , respectively. The authors<sup>19</sup> have added to Freund's near-field, dynamic state of stress the second-order term of  $\sigma_{ox}$  which is acting parallel to the direction of crack extension. This dynamic-singular-crack-tip stress field under mixed-mode loading for small  $\theta$  values differs from the corresponding static stress field in that the largest principal singular tensile stress acts parallel to the  $x$  axis, a fact which not only contributes to crack curving but also to dynamic crack branching. Furthermore, this region ahead of the running crack where  $|\sigma_{xx}| > \sigma_{yy}$  increases with increases in crack speed and  $\sigma_{ox}$  even under pure Mode II crack-tip deformation.<sup>19</sup> This inevitable involvement of  $\sigma_{ox}$  forms the basis of incorporating  $\sigma_{ox}$  in the dynamic-crack-curving criteria presented in this paper.

### Maximum Circumferential-stress Theory

The angle,  $\theta_c$ , at which circumferential stress,  $\sigma_{\theta\theta}$ , is maximum, can be obtained from the following

M. Ramulu (SESA Member) is Research Assistant Professor and A.S. Kobayashi (SESA Fellow) is Professor, University of Washington FU-10, Department of Mechanical Engineering, Seattle, WA 98195.

Paper was presented at SESA Spring Meeting held on Oahu and Maui, HI on May 24-28, 1982.

Original manuscript submitted: November 11, 1981. Authors notified of acceptance: June 21, 1982. Final version received: April 19, 1982.

\*The superscript 'dyn' to identify dynamic-stress-intensity factor will not be used in this paper, since all quantities refer to dynamic values.

$$\frac{\partial \theta_{\theta\theta}}{\partial \theta} = 0 \quad \sigma_{\theta\theta} > 0 \quad (1)$$

where the added  $\sigma_{\theta\theta} > 0$  is to assure fracture in tension under mixed-mode loading.\* For a pure Mode I dynamic-crack-tip state of stress eq (1) will yield a transcendental relation between the critical values of  $\theta$  and  $r$ .

$$r = \frac{1}{4\pi} \left[ \left( \frac{K_I}{\sigma_{ox}} \right) V(\theta, c, c_1, c_2) \right]^2 \quad (2a)$$

Furthermore, by setting  $\theta = 0$  in eq (2a), we obtain

$$r_0 = \frac{1}{128\pi} \left[ \left( \frac{K_I}{\sigma_{ox}} \right) V_0(c, c_1, c_2) \right]^2 \quad (2b)$$

and

$$V_0(c, c_1, c_2) = [B_1(c) \{ -(1 + S_2^2)(2 - 3S_1^2) - \frac{4S_1S_2}{1 + S_2^2} (14 + 3S_2^2) - 16S_1(S_1 - S_2) + 16(1 + S_1^2) \} ] \quad (2c)$$

where

$$B_1(c) = \frac{(1 + S_2^2)}{[4S_1S_2 - (1 + S_2^2)^2]} \quad (2d)$$

$$S_1^2 = \left[ 1 - \frac{c^2}{c_1^2} \right], \quad S_2^2 = 1 - \left[ \frac{c^2}{c_2^2} \right] \quad (2e)$$

and  $c$ ,  $c_1$  and  $c_2$  are the crack velocity, dilatational wave velocity, and distortional wave velocity, respectively. It can be easily shown that for zero crack velocity or  $c = 0$ , eq (2b) reduces to Streit and Finnie's solution<sup>4</sup> of  $r_0 = \frac{9}{128\pi} \left( \frac{K_I}{\sigma_{ox}} \right)^2$ .

\*The exact form of eq (1) is too lengthy to reproduce here but can be found in Ref. 20.

Directional 'instability' is assumed to occur when the running crack deviates from its straight path at  $r_0 \leq r_c$ . Furthermore,  $r_c$  is assumed to be a material constant which can be determined experimentally by using eq (2b).

Figure 1 shows the velocity effect on  $r_0$  which is plotted in a nondimensional form of  $\left[ \sqrt{r_0} \frac{\sigma_{ox}}{K_I} \right]^2$  for Mode I crack extension. Note that the dynamic  $r_0$  is always less than the corresponding static  $r_0$  for crack velocity of  $0 < c \leq 0.325$  and is independent of the sign of  $\sigma_{ox}$ . The terminal crack velocity of  $c/c_1 = 0.325$ , in Fig. 1 where  $r_0 = 0$  coincides with the terminal crack velocity predicted by Yoffe.<sup>15</sup>

### Minimum Strain-energy-density Theory

According to this theory, the crack will extend to the location of the minimum strain-energy-density factor,  $S_{min}$ , or

$$\frac{\partial S}{\partial \theta} = 0 \text{ at } \theta = \theta_c \quad (3)$$

The intensity of the strain-energy density,  $S$ , for the state of plane strain can be written as

$$S = r_0 \frac{(1 + \nu)}{2E} [(1 - \nu)(\sigma_{xx}^2 + \sigma_{yy}^2) - 2\nu(\sigma_{xx}\sigma_{yy}) + 2\sigma_{xy}^2] \quad (4)$$

where  $E$  and  $\nu$  are the modulus of elasticity and Poisson's ratio, respectively. Substituting the dynamic-mixed-mode crack-tip stresses into eq (4) another lengthy equation relating  $K_I$ ,  $K_{II}$ ,  $\sigma_{ox}$ ,  $r$  and  $\theta$  is obtained.<sup>20</sup> Solving for  $r$  results in a transcendental relation, between  $r$  and  $\theta$ , which varies with crack velocity.

By setting the Poisson's ratio  $\nu = 1/3$ , and  $\sigma_{ox} = 0$  as the crack velocity  $c \rightarrow 0$  in eq (3), the static angular prediction of crack curving described in Ref. 13 is recovered. When a nonvanishing second-order term of  $\sigma_{ox}$  is considered, eq (3) yields four  $\theta_c$  values, a pair for  $S_{max}$  and another pair of  $S_{min}$  for given values of  $c$ ,  $K_{II}/K_I$ ,  $r_0$  and

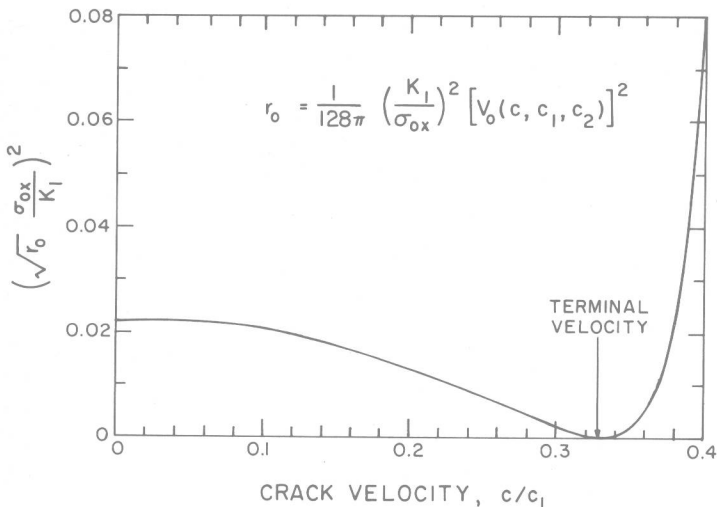


Fig. 1—Nondimensionalized remote stress vs. velocity for Mode I crack extension



$\sigma_{ox}$ . Only the negative root of  $\theta_c$  corresponding to positive  $K_{II}/K_I$  and the positive root of  $\theta_c$  for negative  $K_{II}/K_I$ , under the tensile  $\sigma_{\theta\theta}$  are of interest.<sup>13</sup>

Actual evaluation of eq (3) will show that curving of a straight crack propagating at the lower velocity can be considered only by incorporating the nonsingular term of  $\sigma_{ox}$  in the minimum strain-energy-density criteria. Such possibility of crack curving without  $K_{II}$  values and under the minimum strain-energy criterion has not been considered by others.

### Comparison of Maximum $\sigma_{\theta\theta}$ and Minimum S Criterion

Figure 2 shows the predicted crack-curving angles for crack velocities,  $0 \leq c/c_1 \leq 0.25$  by the maximum circumferential stress and the minimum strain-energy-density criteria with  $\sigma_{ox} = 0$ . Without the second-order term, both criteria predicted the same crack-curving angles for much of the crack-velocity range. Figure 2 also shows that for lower crack velocities of  $c/c_1 \leq 0.15$ , the predicted crack-curving angle, which is referred to as fracture angle from hereon, is almost equal to corresponding static fracture angles.

The effects of the nonsingular term of  $\sigma_{ox}$  and reference distance  $r_0$ , on the fracture angle predicted by both maximum  $\sigma_{\theta\theta}$  and minimum S criteria at various crack velocities are shown in Fig. 3 for  $\nu = 1/3$ , and  $K_{II}/K_I = -0.1$  and  $\sigma_{ox}/K_I = -1.0$  and  $1.0$ . Note that fracture angle for negative  $\sigma_{ox}$  is much smaller than those with positive  $\sigma_{ox}$ . Also, for a given tensile or compressive  $\sigma_{ox}$  larger  $r_0$  results in larger fracture angle. Differences in fracture angles predicted by maximum circumferential-stress theory and minimum strain-energy-density theory

increase with increased  $r_0$  and crack velocity. Reference 14 discusses the influence of  $r_0$  on the fracture angles.

## Experimental Verification

### Dynamic Isochromatics

For a single, pure Mode I or combined Modes I and II crack propagating at a constant velocity, the dynamic crack-tip isochromatic patterns together with the predicted path are shown in Fig. 4. Changes in the remote stress,  $\sigma_{ox}$ , result in backward or forward tilting of the dynamic isochromatics. For a given  $\sigma_{ox}$ , the change in the sign of  $K_{II}$  results in a mirror image change in isochromatics. Detailed discussion of the changes in dynamic isochromatics with variations in  $K_{II}/K_I$  and  $\sigma_{ox}/K_I$  can be found in Ref. 19.

### Data-reduction Procedure

Dynamic isochromatics surrounding a running crack often exhibit moderate unsymmetry. Such photoelastic patterns were heretofore considered experimental abnormalities and were ignored by averaging the unsymmetric patterns during the data-reduction process. Careful postmortem inspection of the fracture specimens, however, show that higher  $\sigma_{ox}$  and slightly unsymmetric isochromatics are often associated with slightly curved crack patterns. With the development of a data-reduction procedure<sup>19,21</sup> for evaluating dynamic  $K_{II}$  together with  $K_I$  and  $\sigma_{ox}$ , it became possible to investigate the above criteria by extracting  $K_I$ ,  $K_{II}$  and  $\sigma_{ox}$  from the previously recorded dynamic isochromatics surrounding running crack tips of curved cracks.

The dynamic-crack-curving criteria developed for pure Mode I loading conditions require accurate determination of  $K_I$  and  $\sigma_{ox}$ . Accuracy of the data-reduction procedure

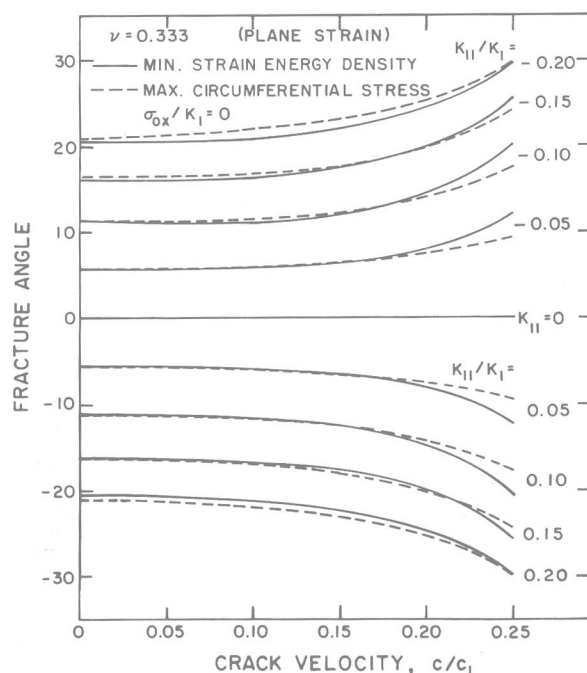


Fig. 2—Fracture angle predicted by maximum circumferential-stress criterion and minimum strain-energy-density criterion,  $\sigma_{ox} = 0$

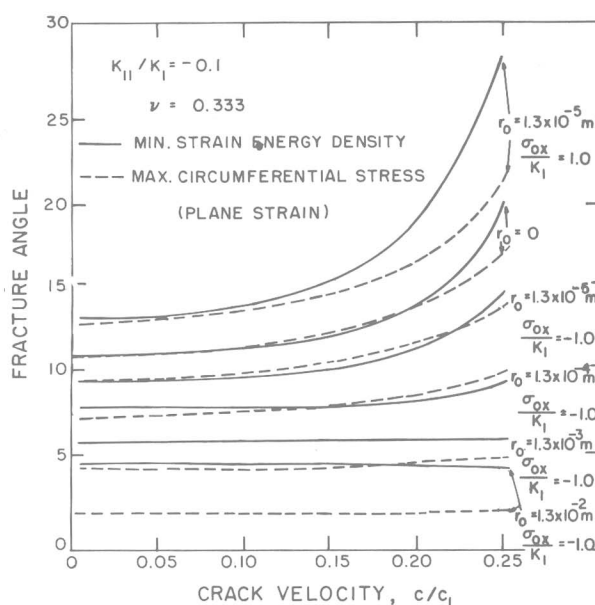
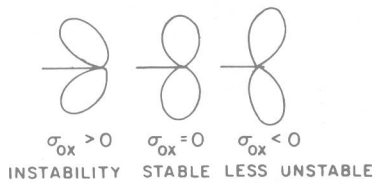


Fig. 3—Effects of  $r_0$  and  $\sigma_{ox}$  on fracture angle  $K_{II}/K_I = -0.1$

CRACK INSTABILITY BY DYNAMIC PHOTOELASTICITY  
UNDER PURE MODE I CONDITIONS



FRACTURE PATH PREDICTIONS BY DYNAMIC PHOTOELASTICITY  
UNDER MIXED MODE CONDITIONS

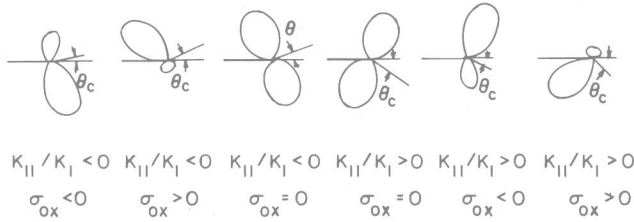
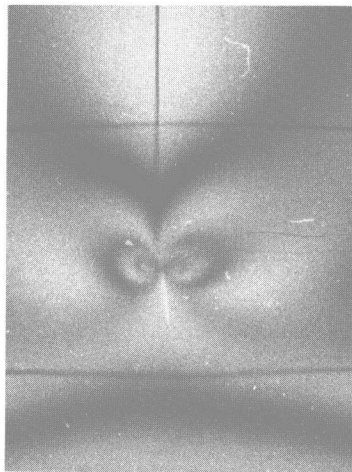
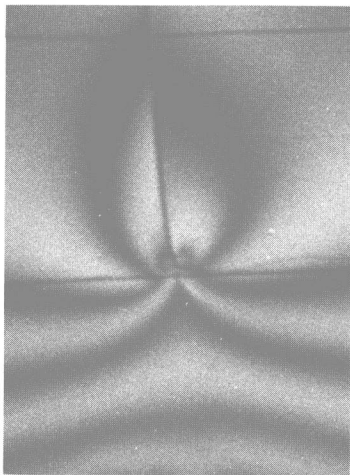


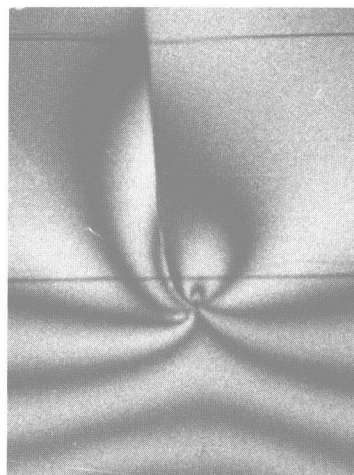
Fig. 4—Expected fracture paths by dynamic photoelasticity



(d) FIFTH FRAME 100  $\mu$  SECONDS  
THEORETICAL ANGLE, 0°; MEASURED ANGLE, 0°



(b) EIGHTH FRAME 130  $\mu$  SECONDS  
THEORETICAL ANGLE, 11°; MEASURED ANGLE, 11°



(c) TENTH FRAME 160  $\mu$  SECONDS  
THEORETICAL ANGLE, 23°; MEASURED ANGLE 26°

Fig. 5—Typical dynamic isochromatics of a curved-crack Homalite-100 dynamic-tear-test (DTT) Specimen No. 6-C051074

used in this investigation was verified by using the above data-reduction procedure to calculate  $K_I$  and  $\sigma_{ox}$  from numerically generated isochromatics using the three parameters of  $K_I$ ,  $\sigma_{ox}$ , and  $A_3$  with  $K_{II} = 0$ .<sup>22</sup> The recovered two dynamic parameters  $K_I$  and  $\sigma_{ox}$  agreed within  $\pm 0.5$  percent and  $\pm 5$  percent, respectively, with the generated results. This series of numerical experiments showed that the two-parameter characterization procedure involving  $K_I$  and  $\sigma_{ox}$  describe reasonably well the stress field in the vicinity of a running crack tip.

The crack-curving angle was measured along the crack path by averaging the measured crack-curving angle at the front and back surfaces of the fractured specimen since the crack surfaces of some of the curved cracks were not perpendicular to the specimen surfaces. The maximum variation between the front and back crack-curving angles was about three degrees for severely curved cracks. Similar differences in out-of-phase crack curving were also observed by Williams *et al.* in their PMMA specimens.<sup>2</sup>

## Results

Figure 5 shows three frames out of a 16-frame dynamic-photoelastic record of a curving crack in a Homalite-100 dynamic-tear-test (DTT) specimen of 9.5-mm (3/8-in.) thick, 88.9 × 400 mm (3½ × 15 in.). This beam with a blunt initial crack of 6.4-mm (7/32-in.) length was impact loaded by a drop weight of 1.48 kg (3.25 lb).<sup>23</sup> The crack emanated from the blunt saw-cut crack and propagated through much of the height of the beam prior to curving near the region of impact loading. Further details of the experimental setup, crack-velocity measurements and dynamic calibration of the Homalite-100 material used are found in Ref. 23. Figure 6 shows  $K_I$ ,  $K_{II}$ ,  $\sigma_{ox}$  and  $r_0$ , which is computed by eq (2), obtained from the dynamic-photoelastic pattern preceding and immediately after crack curving in Fig. 5.  $K_{II}$  is negligible at the point of instability and pronounced fluctuation in  $\sigma_{ox}$  is noted. After crack curving,  $K_{II}$  and  $\sigma_{ox}$  increased while  $K_I$  and the crack velocity dropped rapidly.  $r_0$  was close to 1.5 mm in the continuously curving crack and reached a minimum

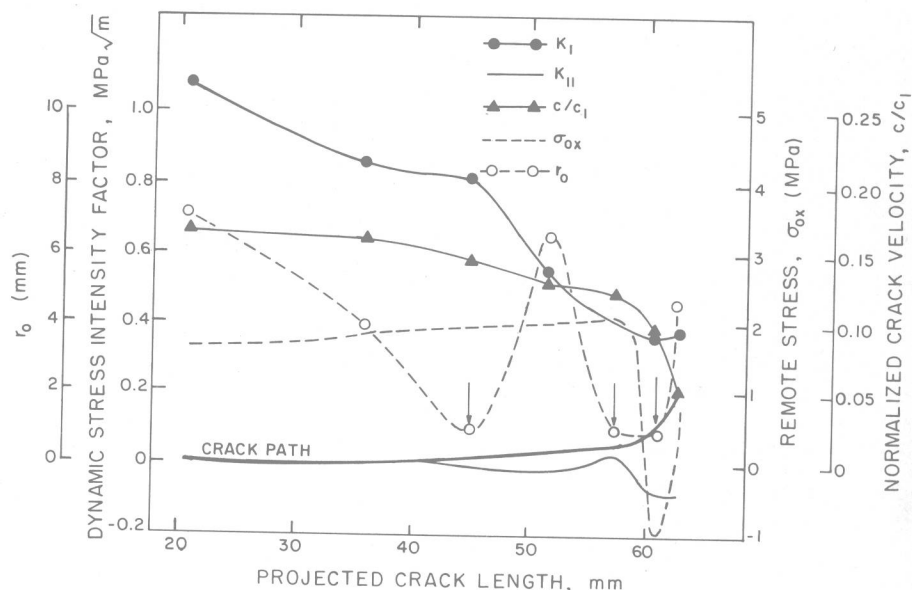
value of  $r_c \approx 1$  mm during the critical stage of crack curving.

Figure 7 shows a slightly curved crack and the associated  $K_I$ ,  $K_{II}$ ,  $\sigma_{ox}$  and  $r_0$  in a fracturing 9.5-mm (3/8-in.) thick, 254 × 254 mm (10 × 10 in.) single-edged-notch (SEN) Homalite-100 specimen.<sup>24</sup> Gradual increase and decrease of  $K_I$ , a small  $K_{II}$  and rapid fluctuations in  $\sigma_{ox}$  and  $r_0$  are noted. In the three SEN test results evaluated,  $K_I$  consistently reached a maximum value prior to crack curving,  $K_{II}$  was negligible and  $\sigma_{ox}$  always increased. At the onset of instability,  $K_I$  suddenly dropped,  $K_{II} = 0$  and  $\sigma_{ox}$  increased.  $r_0$  dropped sharply to an average value of 1.5 mm in all the three SEN-specimen data evaluated at the point of instability. This minimum  $r_0$  value will be referred to  $r_c$  which will be found to be a material parameter associated with dynamic crack curving. A small  $K_{II}$  coexists immediately after crack instability, and changes the direction of crack propagation. A negative  $K_{II}$  immediately after instability resulted in a positive angle of crack curving. This result is not only in agreement with the analytically predicted angles in Fig. 3 but is also in agreement with similar observations in crack curving under stable-crack-growth conditions.<sup>25</sup> The rapid oscillations of  $r_0$  in all the three SEN specimens appeared to be related to the rapid but opposing oscillations in  $\sigma_{ox}$ .

Figure 8 shows a curved crack and the associated  $K_I$ ,  $K_{II}$ ,  $\sigma_{ox}$  and  $r_0$  in a Homalite-100, wedge-loaded, rectangular double-cantilever-beam (WL-RDCB) specimen of 9.5-mm (3/8-in.) thick and 76.2 × 152.4 mm (3 × 6 in.) with a blunt initial crack of length 2.4 mm (0.093 in.). Experimental details of this series of tests can be found in Ref. 26. Fluctuations in dynamic fracture parameters  $K_I$ ,  $K_{II}$ ,  $\sigma_{ox}$  and  $r_0$  are noted all along the curved crack path. Immediately after the instability, a positive small  $K_{II}$  associated with the large  $K_I$  resulted in a negative crack-curving angle. The crack curved continuously without any kinks and is characteristic of the fracture path in a DCB specimen.

Figure 9 shows five frames out of a 16-frame dynamic-photoelastic record of a curving crack in a 9.5-mm (3/8-in.) thick, 254 × 254 mm (10 × 10 in.) Homalite-100

Fig. 6—Dynamic-fracture parameters associated with curved crack shown in Fig. 5





single-edge-notch (SEN) specimen loaded under fixed-gripped tension. The crack emanated from a small pre-crack  $150\ \mu\text{s}$  after impact by a flat-nosed projectile. The severe stress-wave reflections in this specimen caused the crack to curve continuously in a zig-zag manner. Details of this experiment can be found in Ref. 27. Figure 10 shows the corresponding  $K_I$ ,  $K_{II}$ ,  $\sigma_{ox}$  and  $r_0$  variations associated with the unsymmetric dynamic isochromatics in this test. Severe stress-wave loading generated positive  $K_{II}$  and caused the crack to curve immediately after propagation.  $r_c$  is about 1.4 mm but  $\sigma_{ox}$  changed signs, resulting in a zig-zagged crack path.

Fracture angles of curved cracks measured in nine dynamic photoelasticity tests and the corresponding fracture angles computed by the maximum  $\sigma_{\theta\theta}$  and minimum  $S$  theories are summarized in Table 1. Also, theoretically predicted and measured crack-curving angles are shown in Figs. 5 and 9, respectively. The remarkable agreements in experimentally measured and numerically computed results by both theories, using the experimentally determined  $r_c \approx 1.3\ \text{mm}$  for Homalite-100, are noted. Crack-curving angles in our Mode I loading-condition experiments ranged between  $\pm 25\ \text{deg}$  to a minimum of  $2\ \text{deg}$  for severe to moderate curving.

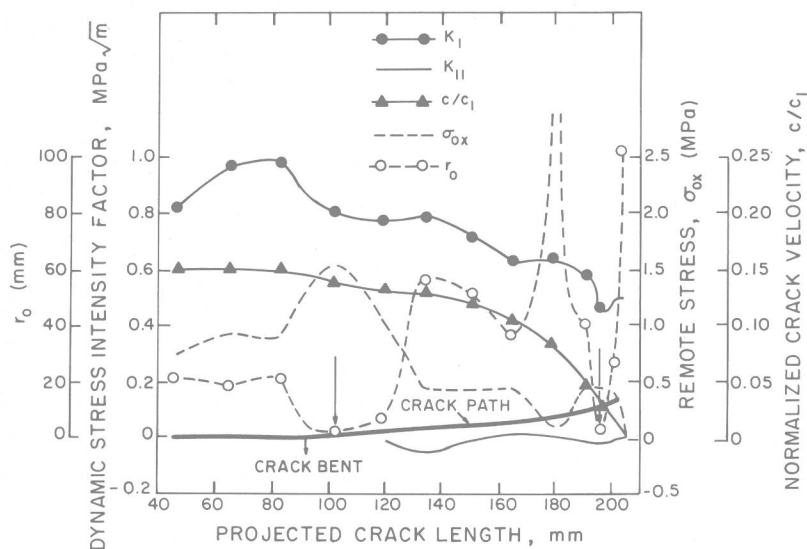


Fig. 7—Dynamic-fracture parameters associated with a slightly curved crack in a single-edge-notch (SEN) tension plate, Homalite-100, Specimen No. B12

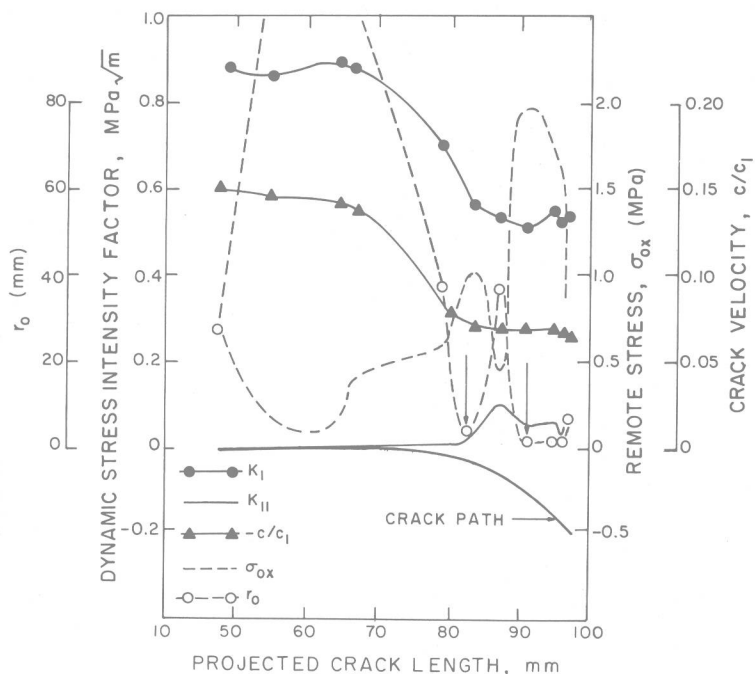


Fig. 8—Dynamic-fracture parameters associated with a curved crack in a wedge-loaded rectangular-double-cantilever (WL-RDCB) specimen, Homalite-100, Specimen No. L7B-051573

Fig. 9—Typical dynamic isochromatics of a curved crack. Homalite-100 single-edge-notch (SEN) specimen impacted by a flat-nose projectile, Specimen No. 21-W090771

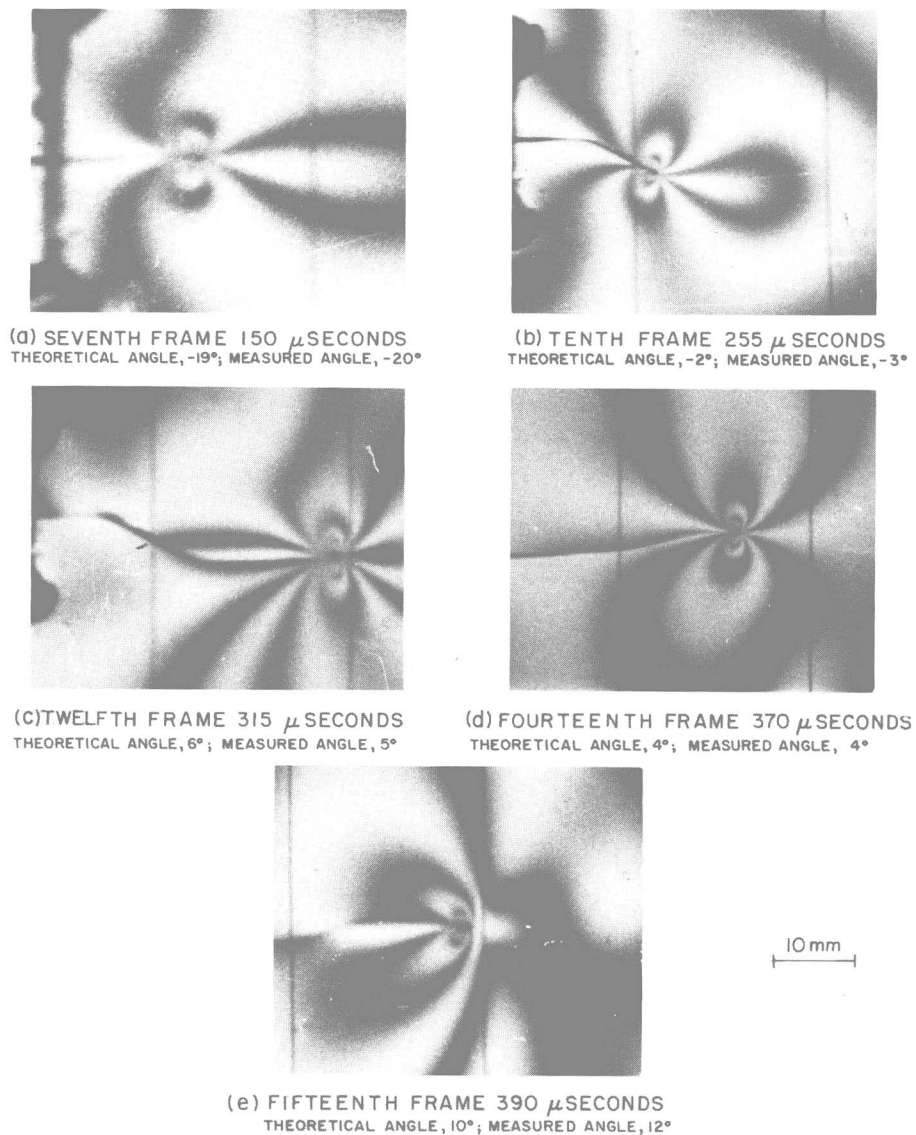
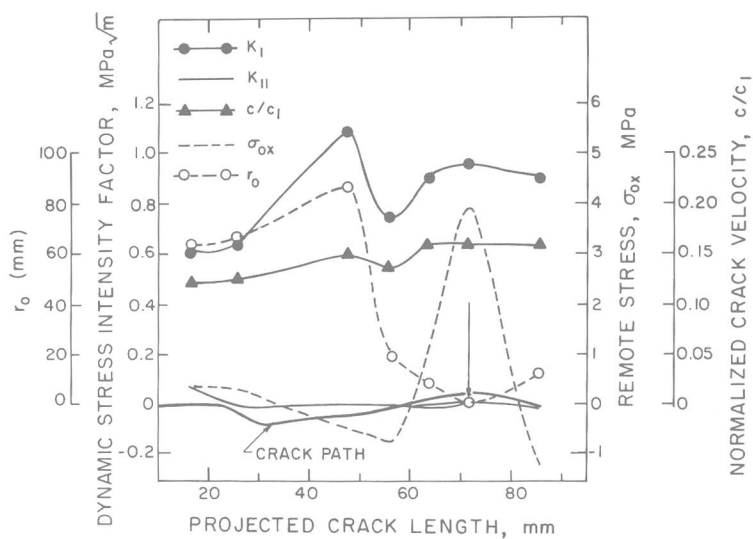


Fig. 10—Dynamic-fracture parameters associated with a curved crack shown in Fig. 9



## Discussion

The closed-form elasticity solution for a circular-arc crack under uniform stress field provides a simple check on the accuracy of using the near-field solution of a straight crack in the results cited above. The static solution given by Panasyuk and Brezhnitskiy<sup>28</sup> in the vicinity of a circular-arc crack with an included angle  $2\alpha$  differ with straight-crack solution only by a multiplication factor of

$$K_I^{\text{curved}} = K_I^{\text{straight}} \cos \alpha / (1 + \sin^2 \alpha / 2) \quad (6a)$$

$$K_{II}^{\text{curved}} = K_{II}^{\text{straight}} \sin \alpha / (1 + \sin^2 \alpha / 2) \quad (6b)$$

$$\sigma_{ox}^{\text{curved}} = \sigma_{ox}^{\text{straight}} \sin^2 \alpha / (1 + \sin^2 \alpha / 2) \quad (6c)$$

where the superscripts 'straight' and 'curved' refer to

TABLE 1—SUMMARY OF EXPERIMENTAL AND THEORETICAL RESULTS

Total number of experiments:	9
Type of fracture specimen:	DTT, SEN, WL-RDCB
Number of data points:	81
Crack velocity, $c/c_1$ :	0.03 to 0.21
$K_I$ (MPa $\sqrt{\text{m}}$ )	0.50 to 1.59
$K_{II}/K_I$	-0.22 to 0.18
$\sigma_{ox}/K_I$	-2.89 to 4.04
Experimental fracture angle associated with crack curving:	-20 deg to 26 deg
Theoretical prediction of fracture angle:	-20 deg to 25 deg
$r_c$ (mm)	1.0 to 1.5

crack-tip parameters associated with a straight and curved crack, respectively. Possible errors, which were generated by fitting a straight-crack solution to a curved crack, were estimated. The procedure consisted of least-square fitting the exact solution of a curved crack and the corresponding solution for a straight crack to the two extreme curved cracks associated with the latest data points in Figs. 6 and 8. The resultant  $K_I$ ,  $K_{II}$  and  $\sigma_{ox}$  of the straight-crack solutions are within 10 percent, 28 percent and 6 percent, respectively, of the corresponding solutions for circular-arc cracks of  $\alpha = 25$  and 28 deg. Thus, possible error introduced by using a second-order dynamic-crack-tip state of stress of a straight crack in place of a curved crack should be negligible for most of the curved-crack problems of  $\alpha = 5$  and 10 deg in this investigation.

Figure 11 illustrates the influence of  $\sigma_{ox}$  on the shape and tilting of the isochromatics. For a given  $K_{II}/K_I = 0.1$  and crack velocity of  $c/c_1 = 0.16$ , a -0.1 to 0.1 variation in  $\sigma_{ox}/K_I$  will result in a six-percent variation in the maximum radial distance,  $r_{max}$ , and a  $\pm 12$ -percent variation in the angle of tilt,  $\theta_m$ , of the isochromatics. Conversely, should  $r_{max}$  and  $\theta_m$  be measured within  $\pm 6$  percent and  $\pm 12$  percent, a range of  $-0.1 < \sigma_{ox}/K_I < 0.1$  is to be expected.

Figure 12 shows an enlarged figure of the fifteenth frame of the recorded isochromatic patterns associated with the curved crack of Fig. 9.  $K_I$ ,  $K_{II}$  and  $\sigma_{ox}$  were determined from isochromatic-fringe order of 3.5 for the curved crack. The accuracy in  $\sigma_{ox}$  determination can be estimated by comparing the calculated and recorded fringes of order 2.5. The coincidence is reasonable for a radial distance of about 5 mm (0.2 in.) and thus the error involved in  $\sigma_{ox}$  estimation is negligible.

The developed dynamic-crack-curving criterion shows that the large  $\sigma_{ox}$  contributes to crack instability and is in agreement with Benbow and Roessler's conclusion involving static experiments.<sup>29</sup> Cotterell<sup>30-32</sup> referring to Williams's

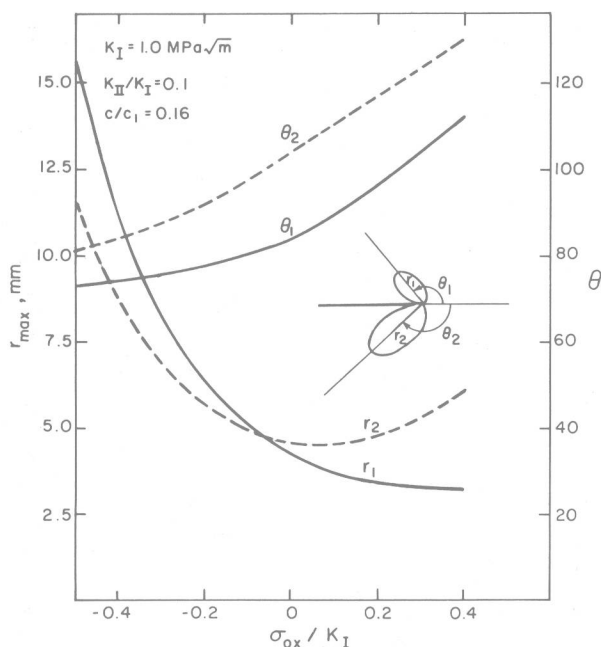


Fig. 11—Effect of  $\sigma_{ox}$  on the isochromatic fringe

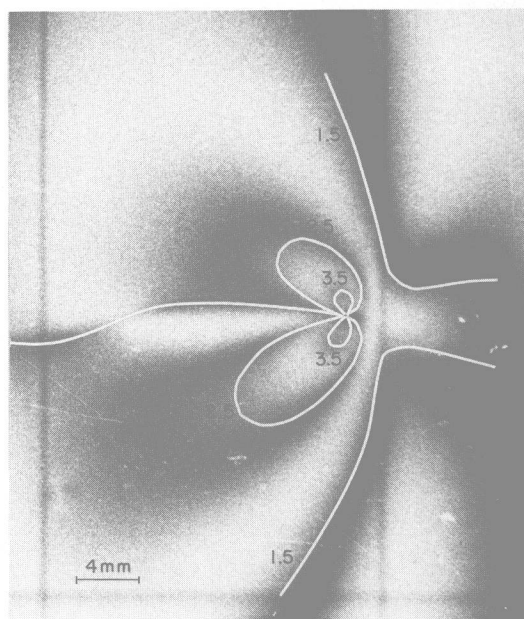


Fig. 12—Calculated and recorded isochromatics, 15th frame, 390  $\mu\text{s}$  of Fig. 9



analysis,<sup>33</sup> showed that the crack path will be unstable when  $\sigma_{ox}$  is positive. The above static-crack-stability criterion<sup>29-32</sup> correlates well with the experimental results of DCB and CT specimens but cannot explain dynamic crack curvings in fracture specimens of SEN, and DTT where  $\sigma_{ox}$  is negative. The proposed criterion for the directional stability of a propagating crack is independent of the sign of the  $\sigma_{ox}$ , and is thus applicable to all crack-curving data considered in this paper.

As shown in Fig. 3 the influence of nonsingular stress is more pronounced for moderate values of  $r_0$  irrespective of the sign of  $K_{II}/K_I$ . This result re-emphasizes the importance of the nonsingular stress term  $\sigma_{ox}$ , which, when neglected, can lead to inaccurate results as observed by Tirosh.<sup>34</sup>

Considering the fact that dynamic photoelasticity experiments cited in this paper were conducted by four different investigators over a period of ten years with different shipments of Homalite-100, the consistent results of  $r_c = 1.3$  mm is noticeable. This magnitude of  $r_c$  at the onset of stability is larger than those reported in Refs. 2 and 11, which is due partly to the different material under consideration but mainly due to the ad hoc procedure in which  $r_c$  values were determined by others. In a critical review of  $r_c$  associated with the minimum S criterion of crack curving, Theocaris and Andrianopoulos<sup>14</sup> also determined experimentally  $r_c = 1.3$  mm (0.05 in.) for polymethylmethacrylate.

Finally, the crack-curving criterion by Karihaloo *et al.*<sup>12</sup> requires that  $K_{II}$  be known immediately before and after crack curving. The lack of sensitivity in this analysis precluded precise variations of the very small  $K_{II}$  before or after crack curving and thus this crack curving could not be checked.

## Conclusions

(1) A dynamic-crack-curving criterion based on the directional stability of a running crack at a critical distance

$$r_0 = 1/128 \pi [(K_I/\sigma_{ox}) V_0(c, c_1, c_2)]^2$$

under pure Mode I loading is developed. Directional stability is ensured when  $r_0 > r_c$ , where  $r_c$  is a critical material constant.

(2) Dynamic fracture angle under pure Mode I and mixed Mode I and II conditions can be predicted by using either the maximum circumferential-stress or the minimum strain-energy-density theories with the non-singular stress term  $\sigma_{ox}$ . The difference in dynamic-crack-curving angles predicted by either theories nearly is equal for  $\nu = 0.33$  to those of static analyses when  $c/c_1 \leq 0.15$ .

(3) Positive  $\sigma_{ox}$  always enhances the crack curving and negative  $\sigma_{ox}$  reduces the fracture angle irrespective of the sign of  $K_{II}/K_I$ .

(4) Experimental results with and without  $K_{II}$  proved that  $r_c$  is a material constant. The critical value of Homalite-100 is  $r_c = 1.3$  mm (0.05 in.).

## Acknowledgment

The results reported in this paper were obtained through ONR Contract No. 00014-76-C-0600 NR 64-478. The authors wish to thank N. Perrone and Yapa Rajapakse, ONR, for their support during the course of this investigation.

## References

1. Erdogan, F. and Sih, G.C., "On the Crack Extension in Plates Under Plane Loading and Transverse Shear," *Trans. ASME J. Basic Eng.* **85** (D), 519-527 (1963).
2. Williams, J.G. and Ewing, P.D., "Fracture Under Complex Stress - The Angled Crack Problem," *Int. J. Fract. Mech.*, **8**, 441-446 (1972).
3. Finnie, I. and Saith, A., "A Note on the Angled Crack Problem and the Directional Stability of Crack," *Int. F. Fract.*, **9**, 484-486 (1973).
4. Streit, R. and Finnie, I., "An Experimental Investigation of Crack-path Directional Stability," *EXPERIMENTAL MECHANICS*, **20** (1), 17-23 (Jan. 1980).
5. Cotterell, B. and Rice, J.R., "Slightly Curved or Kinked Cracks," *Int. J. Frac.*, **11** (2), 155-164 (1981).
6. Karihaloo, B.L., Keer, L.M., Nemat-Nasser, S. and Oranratnachai, A., "Approximate Description of Crack Kinking and Curving," *ASME Paper No. 81-APM-22*.
7. Hussain, M.A., Pu, S.L. and Underwood, J., "Strain-Energy-Release Rate for a Crack Under Combined Mode I and Mode II," *ASTM-STP-560*, 2-28 (1974).
8. Palaniswamy, K. and Knauss, W.G., "On the Problem of Crack Extension in Brittle Solids Under General Loading," *Mechanics Today*, **4**, ed. S. Nemat-Nasser, Pergamon Press, 87-148 (1978).
9. Gupta, G.D., "Strain Energy Release Rate for Mixed Mode Crack Problem," *ASME Paper No. 76-WA/PVP-7*.
10. Wu, C.H., "Elasticity Problems of Slender Z-Crack," *J. Elasticity*, **8**, 183-205 (1978).
11. Hayashi, K. and Nemat-Nasser, S., "Energy Release Rate and Crack Kinking," *Int. J. of Solids and Structures*, **17**, 107-114 (1981).
12. Karihaloo, B.L., Keer, L.M. and Nemat-Nasser, S., "Crack Kinking Under Non-Symmetric Loading," *Engrg. Fract. Mech.*, **13**, 879-888 (1980).
13. Sih, G.C., "A Special Theory of Crack Propagation," *Methods of Analysis and Solutions of Crack Problems*, **1**, ed. G.C. Sih, Noordhoff Inter. Publishing, Leyden, 21-45 (1973).
14. Theocaris, P.S. and Andrianopoulos, N.P., "A Modified Strain Energy Density Criterion Applied to Crack Propagation," *J. Appl. Mech.*, **49** (1), 81-86 (1982).
15. Yoffe, E.H., "The Moving Griffith Crack," *Phil. Mag.*, **42**, 739-750 (1951).
16. Sih, G.C., "Dynamic Crack Problems: Strain Energy Density Fracture Theory," *Elastodynamic Crack Problems*, **4**, ed. G.C. Sih, Noordhoff Inter. Publishing, Leyden, 17-37 (1977).
17. Freund, L.B., "Dynamic Crack Propagation," *The Mechanics of Fracture*, **19**, ed. by F. Erdogan, ASME, 105-134 (1976).
18. Freund, L.B., "The Mechanics of Dynamic Shear Crack Propagation," *J. Geophysical Res.*, **84** (35), 2199-2209 (1978).
19. Kobayashi, A.S. and Ramulu, M., "Dynamic Stress-intensity Factors for Unsymmetric Dynamic Isochromatics," *EXPERIMENTAL MECHANICS*, **21** (1), 41-48 (Jan. 1981).
20. Ramulu, M., "Dynamic Crack Curving and Branching," doctoral thesis submitted to the Univ. of Washington (March 1982).
21. Kobayashi, A.S. and Ramulu, M., "Dynamic Mixed Mode Fracture," *Proc. U.S.-Greece Symp. on Mixed Mode Fracture*, ed. G. Sih and P.S. Theocaris, Noordhoff, Holland (1981).
22. Kobayashi, A.S. and Mall, S., "Dynamic Fracture Toughness of Homalite-100," *EXPERIMENTAL MECHANICS*, **18** (1), 11-18 (Jan. 1978).
23. Kobayashi, A.S. and Chan, C.F., "A Dynamic Photoelastic Analysis of Dynamic-tear-test Specimen," *EXPERIMENTAL MECHANICS*, **16** (5), 176-181 (May 1976).
24. Bradley, W.B. and Kobayashi, A.S., "Fracture Mechanics - A Photoelastic Investigation," *Engrg. Frac. Mech.*, **3**, 317-332 (1971).
25. Iida, S. and Kobayashi, A.S., "Crack Propagation Rate in 7075-T6 Plates Under Cyclic Tensile and Transverse Shear Loading," *J. Basic Engrg.*, *Trans. of ASME*, **91**, Series D (4), 764-769 (Dec. 1964).
26. Kobayashi, A.S., Mall, S. and Lee, M.H., "Fracture Dynamics of Wedge-Loaded Double Cantilever Beam Specimen," *Cracks and Fracture*, *ASTM STP*, **601**, 274-290 (June 1976).
27. Wade, B.G. and Kobayashi, A.S., "Photoelastic Investigation on the Crack Arrest Capability of Pretensioned Stiffened Panels," *EXPERIMENTAL MECHANICS*, **15** (1), 1-9 (1975).
28. Panasyuk, V.V. and Brezhnitskiy, L.T., *Voprosy Mekhaniki, Real nogo Tverdogo Tela No. 3*, Naukova Dumka Press, Kiev (1965).
29. Benbow, J.J. and Roesler, F.C., "Experiments on Controlled Fractures," *Proc. Phys. Soc.*, **70**, Ser. B, 201-211 (1957).
30. Cotterell, B., "Notes on the Paths and Stability of Cracks," *Int. J. Frac. Mech.*, **2**, 526-533 (1966).
31. Cotterell, B., "On Fracture Path Stability in the Compact Tension Test," *Int. J. Frac. Mech.*, **6**, 189-192 (1970).
32. Cotterell, B., "On Brittle Fracture Paths," *Int. J. Frac. Mech.*, **1**, 96-103 (1965).
33. Williams, M.L., "On the Stress Distribution at the Base of a Stationary Crack," *J. Appl. Mech.*, **24**, 109-116 (1957).
34. Tirosh, J., "Incipient Fracture Angle, Fracture Loci and Critical Stress for Mixed Mode Loading," *Eng. Frac. Mech.*, **9**, 607-616 (1977).